Backprojection Autofocus for Synthetic Aperture Radar

Michael I Duersch and David G Long

Department of Electrical and Computer Engineering, Brigham Young University

***Abstract*—In synthetic aperture radar (SAR), many adverse conditions may cause errors in the raw phase-history data. Autofocus methods are commonly used in SAR to mitigate the effects of these problems. Over the years, many types of autofocus have algorithms have been created, however, each has implicit assumptions restricting their use. The backprojection image formation algorithm places few restrictions on SAR imaging, thus it is desirable to have an autofocus algorithm that is similarly unconstrained. This paper presents a versatile autofocus method that is accordant with backprojection.**

***Index Terms*—synthetic aperture radar (SAR), backprojection, autofocus.**

I. Introduction

Autofocus algorithms are commonly employed in synthetic aperture radar (SAR) to remove phase errors due to uncompensated motion, atmospheric propagation effects, hardware limitations, or processing approximations. These phase errors have varying effects on image quality depending on the nature of the errors. All share the commonality that they reduce image focus.

Autofocus techniques typically fall into two categories: *model* based and *estimation* model based [1]. Model based autofocus methods estimate a set of coefficients that parameterize a model which is used to compensate for phase errors. Estimation based methods estimate a phase function which is used to compensate for phase errors.

Many autofocus methods have been developed for SAR. Some of the more common methods are map-drift autofocus (MDA) [2], phase-gradient autofocus (PGA) [3], [4], and prominent point processing (PPP) [5].

The map-drift autofocus methods are model based and operate by forming two or more subaperture images for a given scene. The necessary translation required to register the images is used to estimate coefficients in the phase correction model. If a scene is divided into two subapertures then a quadratic phase error estimate results. Increasing the number of subapertures yields higher order estimates. MDA is thus able to provide an accurate compensation but only for low-order phase errors since it is limited to estimating a small number of parameters.

Phase-gradient autofocus is an estimation based method. In it, an isolated bright target is taken at each range gate. The phase characteristics of each target are examined and averaged together from which the phase correction function is estimated. PGA has the advantage that it is able to accurately estimate high-order phase errors. However, it also has restrictions on imaging geometry and requires isolated, bright targets in the scene at various ranges. Targets with low SNR or that are two close together can present difficulties.

Prominent point processing is an estimation method that measures the pulse-to-pulse range and phase variations of several prominent point targets in a scene. Thus, it is able to accurately estimate low and high-order phase errors. It is also able to measure rotational motion in SAR/ISAR collections. Its drawbacks are the requirement of prominent, uninterrupted point targets for phase and range estimation, as well as being potentially interactive (i.e., not strictly *automatic*).

Most autofocus methods assume spotlight-mode imaging where, after polar formatting, an inverse Fourier transform in azimuth yields the original range-compressed data. For stripmap SAR data, a simple inverse transform does not provide this. For example, to apply traditional autofocus methods to a stripmap image requires deconvolving with the azimuth matched filter (i.e., Doppler chirp). This is not well posed as it would be better to operate on each pulse of the range-compressed phase history data prior to image formation.

An additional limitation of most autofocus methods is the requirement of linear platform motion. This arises because of the assumption of a linear FM Doppler chirp in the range compressed data to estimate phase errors. Large, uncompensated motion or more exotic flight geometries (i.e., circular SAR) pose problems for traditional autofocus algorithms. As the backprojection image formation algorithm is unconstrained, it is desirable to have an autofocus that similarly unconstrained.

Section II-A presents a brief overview of the backprojection image formation algorithm, followed by common sources of phase error in Section II-B. Section III introduces the autofocus methodology. Finally, Section IV shows results for simulated and experimental data.

II. Background

Before presenting our approach to autofocus, we begin by describing the BP image formation algorithm. Following that, we list common sources of phase error for SAR with backprojection.

A. Backprojection Algorithm

The backprojection method forms images from input range-compressed SAR data, and may be thought of as the ideal matched filter. Because image formation occurs in this domain no assumptions of flight motion are required. Thus, the data input to the image formation algorithm need not be regularly sampled nor motion compensated. The key is that the flight motion be known precisely. In order to motivate the autofocus

method presented later, we begin with a brief mathematical description of the backprojection algorithm. The complete backprojection derivation appears in [6].

For this analysis, we begin with a general, range-compressed SAR signal. In this context, range compression means matched filtering the received pulses with their transmit waveform. It is assumed that distances are large enough that the plane-wave approximation may be used. In order to simplify analysis, a stop-and-go transmit/receive approximation is also used.

Given the above assumptions, a general expression for the range-compressed signal from a stationary isotropic point scatterer may be given by

$$s_p(l) = \sigma\, \alpha_p R(l - d_p) e^{-jkd_p} \tag{1}$$

where p is the pulse number (discrete time), l is fast-time (in distance) relative to the beginning of the pulse (continuous time), σ is the backscatter radar cross-section of the point scatterer, α_p includes all gain terms, k is the wavenumber of the carrier signal ($k = \frac{2\pi}{\lambda}$, λ is the wavelength), $R(l)$ is the range compressed radar response including range windowing, and d_p is the two-way distance traveled by the radar signal. Note that $l = c\,t$ where c is the propagation speed and t is fast-time. The mapping from time to distance is for convenience. Thus, the signal from the scatter is a function of pulse index (i.e., slow-time) and propagation distance (i.e., fast-time).

The scatterer reflections are present in a series of pulses as the platform travels. In forming an image, it is desirable to focus this energy as narrowly as possible. This process is termed *slow-time compression* or *azimuth compression*.

In order to focus a target's energy in azimuth, its contribution from each of the sequential pulses must be combined. The process of matched filtering, or cross-correlating a signal with with its template, achieves this in a coherent fashion. Matched filtering also has the advantage of maximizing SNR [7]. The azimuth matched filter for $s_p(l)$ above is

$$h_p = e^{-jk\tilde{d}_p}, \tag{2}$$

where $\tilde{d}_p$ is the distance at each pulse parameterizing the matched filter.

The process of slow-time (azimuth) matched filtering is performed by cross-correlating $h_p(t)$ with the original signal $s_p(t)$ and results in the matched filtered signal

$$\begin{aligned} f_q(l) &= \sum_{p\in\mathcal{P}} h_p^*(l) s_{p+q}(l) && (3)\\ &= \sigma \sum_{p\in\mathcal{P}} \alpha_p R(l - d_p) e^{-jk\left(d_p - \tilde{d}_p\right)}, && (4) \end{aligned}$$

where $\mathcal{P}$ is the set of all pulses contributing to the target. For the sake of brevity, we skip the intermediate steps to give the result at the point of zero shift ($q = 0$, $l = 0$) when the matched filter distance equals the actual distance to the target:

$$a_0 = f_0(0) = \sigma R(0) \sum_{p\in\mathcal{P}} \alpha_p, \tag{5}$$

where a_0 is the backprojected pixel value.

This is the ideal range and azimuth compressed pixel value for a single point target inside a scattering cell whose position is precisely known. Note that throughout the analysis we use the term *pixel* to refer to the imaged signal and *scattering cell* to refer to the physical location being imaged.

The pixel value a_0 resulting from Eq. (5) assumes that the phase of the matched filter perfectly matches the geometric phase of the signal at each pulse. For this assumption to hold, the target must be located at precisely the anticipated position (i.e., the center of the scattering cell) and the antenna phase center must also be known. We now examine the case where the scatter location is displaced from the anticipated position or the antenna phase center is displaced from the measured position. Let $\delta_p = \tilde{d}_p - d_p$ be the difference in the matched filter distance $\tilde{d}_p$ and the actual distance traveled d_p. Again skipping several steps and assuming δ_p is sufficiently small, this results in

$$\tilde{a}_0 \approx \sigma \sum_{p\in\mathcal{P}} e^{jk\delta_p} \alpha_p R(\delta_p). \tag{6}$$

Note that in this case, as $|R(\delta)| \leq |R(0)|$ with $\delta \neq 0$, and as the residual phase $e^{jk\delta_p}$ exists at each element in the sum, then by the triangle inequality,

$$|\tilde{a}_0| \leq |a_0|. \tag{7}$$

This results in a lower signal magnitude for $\tilde{a}_0$, a property that will be exploited in the autofocus method presented later.

B. Sources of Phase Error

In traditional SAR imaging there are three common sources of phase error: 1. radar system timing errors (including "signal propagation through media with unknown spatially varying propagation velocity" [8]), 2. antenna position measurement errors, and 3. approximations in motion compensation and image formation. In backprojection, we exchange the third error source for an alternate: target location errors. In the following we discuss each error source for backprojection.

1) Radar System Phase Error : As the radar system is dependent on a clock (e.g. local oscillator) that is subject to drift and other effects, the result is small inaccuracies in the measurement of time-of-flight of the pulse. Usually this difference is within a small fraction of a second, but as the period of a wave at the carrier frequency may be nanoseconds or less, any uncertainty may lead to phase errors. For high-altitude SARs, variations in propagation velocity through the atmosphere cause a similar effect. These errors can often be approximated as constant across a given pulse. When this is the case, a single scalar estimate of the phase error is sufficient to compensate for this.

2) Position Measurement Errors: As already shown, the backprojection algorithm operates by calculating the ideal azimuth matched filter from exact knowledge of the range to scattering cell at every pixel in the output image. This dependence on knowledge of range-to-target is common for all SAR image formation algorithms. However, as most others form images in the slant-plane, the range to target implicit in the radar data itself is sufficient for image formation. The backprojection algorithm requires explicit knowledge of the range to target at every pulse. This makes the backprojection

process highly sensitive to errors in antenna position. Thus, precise antenna position measurements are required.

In SAR, this usually calls for use of a high-grade inertial navigation system (INS). An INS incorporates an inertial measurement unit (IMU) which incorporates accelerometers and gyroscopes to measure motion and rotation. A Global Position System (GPS) unit is often included to provide absolute positioning and mitigate measurement drift. While GPS units aren't expensive, precise inertial measurement units (IMU) with low drift unfortunately are expensive. Table I provides general specifications for typical grades of IMU. [1] While lower cost automotive and industrial grade IMUs are available, their performance is not suitable for SAR image formation.

An additional factor limiting image quality is that increasing the flight altitude causes the synthetic aperture to grow longer. This means that if a given IMU has a tolerable amount of drift at one altitude, when the altitude is increased that same IMU may no longer be adequate for image formation. While higher precision (and more expensive) IMUs are available, they are also larger, heavier, and draw more power. This may prohibit their use on smaller unmanned aerial vehicles (UAVs) that have severe payload weight constraints. Because of these constraints, rather than improve INS hardware, it is desirable to develop a signal processing method to increase image quality.

As shown in the Section II-A, the backprojection matched filter is a function of the range to target (pixel or cell) at each slow-time sample. This range may be obtained given the scattering cell location and phase center of the antenna according. Thus, errors in the position estimate of the phase center of the antenna lead to phase errors in the backprojected image. The phase error ϕ_e for a specific antenna and target position as a function of position estimate error is

$$\phi_e \quad = \quad e^{j\,2k\sqrt{\left(x+x^{'}\right)^2+(y+y^{'})^2+(z+z^{'})^2}}, \tag{8}$$

where (x, y, z) are the true coordinates of the the antenna phase center relative to the pixel center and $(x^{'}, y^{'}, z^{'})$ are the measurement errors. This may be approximated as

$$\phi_e \approx \exp\left(j\frac{2k}{r}\left(x^{'}x + y^{'}y + z^{'}z\right)\right) \tag{9}$$

if the measurement errors are small and the azimuth coordinate $x \ll r$ where $r = \sqrt{y^2 + z^2}$, the range at the point of closest approach.

Figure 1 shows the magnitude of the phase error for various geometries as a function of the lateral position error to wavelength ratio (e.g. $y^{'}/\lambda$) . Multiple lines are plotted, each representing a different incidence angle to the target. A horizontal line is placed at $\pi/8$, which serves as a reminder that any phase error above this becomes a source of significant phase error in the backprojection sum.

[1]For our purposes, tactical grade means an accelerometer bias error less than 1 mg.

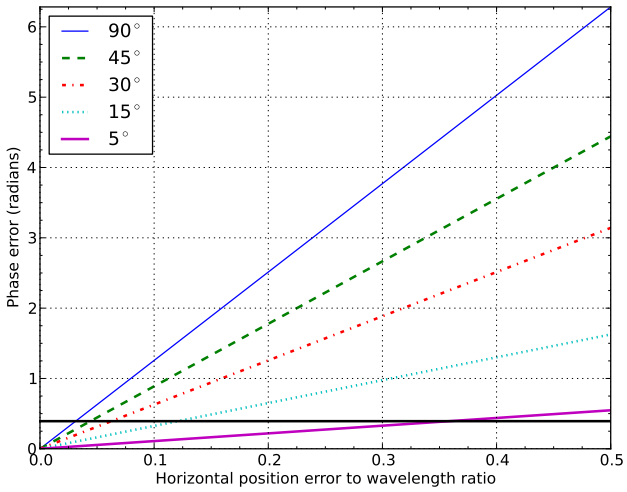

Figure 1. Estimate of the phase error for position estimate errors as a function of the ratio of position error magnitude to wavelength. Multiple lines are shown for various coordinate to slant-range ratios. The horizontal line marks the phase $\pi/8$.

3) DEM Errors: The backprojection formula requires knowledge of the position in three-space of every scattering cell calculated. To aid the backprojection process, a priori knowledge of the cell's vertical position is usually provided via a digital elevation map (DEM) of the imaged terrain. A bias error (i.e., a height offset) in the elevation map results in varying effects in the output image depending on the SAR collection geometry and the exact steps performed in backprojection processing.

For the simplest case, assume that a SAR platform has a straight and level flight track. In this scenario, all of the platform motion is in the along-track direction (i.e., there is no motion in elevation or cross-track). This means that while the slant-range from the SAR to a stationary target on the ground is unique, the ground-range and elevation of the target cannot be uniquely determined. The possible solutions to these parameters lie on a hyperbolic curve, any point of which provides the correct solution of slant-range-to-target distance. Thus, each range/elevation solution produces an equally well focused target in the backprojected image. The position of the target in the output image may be affected, however.

As the azimuth position of the target is uniquely determined for this imaging geometry, an offset in the elevation map does not affect the azimuth position of the target in the backprojected image. The same is not true in the range dimension. Raising the elevation map (i.e., targets are closer to the SAR in elevation) requires that targets appear farther away in ground-range in order to maintain the same slant-range distance. In the same way, lowering the elevation map causes targets to appear closer to the SAR in ground-range. Thus, unless the elevation map specifies the correct terrain height, targets are erroneously shifted in range. It is important to remember, however, that regardless of the shift in range, the target's focus is unaffected.

For the case above, all platform motion is assumed to be in the along-track direction. If any motion occurs in the

Table I
INERTIAL MEASUREMENT UNITS (IMUS)

Grade	**Cost**	**Weight**	**Accelerometer Bias Error**	**Horizontal Position Error** (m)			
		(lbs)	(mg)	1s	10s	60s	1hr
Automotive	$1 - $500	< 0.5	125	620 mm	60 m	2.2 km	7900 km
Industrial	$500 - $3k	< 1	3	15 mm	1.5 m	53 m	190 km
Tactical	$5 - $30k	2.5	0.3	1.5 mm	150 mm	5.3 m	19 km
Navigation	> $100k	> 6	0.025	0.12 mm	12 mm	0.44 m	1.6 km

cross-track or elevation direction then the solution yielding the target position becomes more constrained. Thus, if the correct height for the elevation map is not used then the target's compression suffers. In the stripmap mode however, as the terrain is stationary, this effect is small unless large elevation errors occur. This is because offsetting the target location adds approximately a constant range error at every pulse, and thus approximately the same phase. As the phase added is roughly constant, it has little effect on compression. As the DEM errors grow then the approximation no longer holds.

III. AUTOFOCUS

A. Methodology

As indicated previously, most autofocus methods involve analysis of the formed image (i.e., range and azimuth compressed) in order to estimate proper correction factors. Our method differs in that the autofocus adjustment is calculated on a per-pulse basis prior to image formation. Recall from Eqs. 5 that the maximum pixel magnitude is obtained when the backprojection matched filter uses the exact range-to-target at every pulse in the summation. As shown in Eq. 6 and 7, a distance error reduces the pixel magnitude. This distance error may instead be considered a corresponding phase error. In fact, any and all phase error terms present at each pulse may be lumped into a single value.

The effect of this may be described in an intuitive manner. Each sample from a range compressed pulse is a complex value with contributions from a group of illuminated targets and also contributes to a group of pixels in the output image. This complex value is a vector representing magnitude and phase. The azimuth matched filtering of Eq. 2 represents a rotation of that sample at a given pulse. When perfect matched filtering occurs, all of the sample vectors are rotated to the same direction such that when they are summed, all sum constructively yielding a result with large magnitude and phase equal to the intrinsic phase of the target cell. The errors described earlier distort this process so that each sample no longer adds in phase and a degraded pixel sum results.

Because the matched filtered pulses with phase error do not sum in phase, the backprojection sum yields a lower pixel magnitude. This suggests the simple solution of applying a phase correction to each pulse that maximizes the magnitude of the pixel sum. While this approach works well with isolated, prominent targets, it may not work in general. If multiple "bright" targets are located near the target of interest, their returns may overlay at some pulses. If all the samples are assumed to come from a single source (i.e., the target of interest), then the samples containing the bright returns of nearby objects are erroneously rotated to maximize the pixel magnitude of the target of interest. This can result in target "ghosting" in the output image. Also, because of noise/clutter this may not perform well with lower SNR pixels. It is therefore advantageous to simultaneously focus a group $\mathcal{M}$ of pixels $\left(a_1, a_2, \ldots, a_{|\mathcal{M}|}\right)$. Here, $|\mathcal{M}|$ indicates the cardinality of set $\mathcal{M}$ (i.e., the number of elements in the set).

In order to focus a group of pixels, some kind of optimization method utilizing a cost function is required. The proposed autofocus technique estimates the phase error at each pulse using coordinate descent optimization. A similar approach is taken by [9] for convolution backprojection. The coordinate descent method performs a *line search* at a point along a single coordinate direction for each iteration [10]. In other words, the function $F(\mathbf{x})$ with $\mathbf{x} = \left(x_1, x_2, \ldots, x_{|\mathcal{P}|}\right)$ is minimized one component x_p at a time. After all coordinates have been searched, a single descent iteration $\mathbf{x}^k$ (with iteration index k) is complete. Therefore, beginning with an initial guess $\mathbf{x}^0$ for a local minimum of F, one can iteratively obtain the sequence $\mathbf{x}^0,\ \mathbf{x}^1,\ \mathbf{x}^2,\ \ldots$. This guarantees that at each iteration

$$F(\mathbf{x}^0) \geq F(\mathbf{x}^1) \geq F(\mathbf{x}^2) \geq \ldots \ . \tag{10}$$

The function minimization for each component in $\mathbf{x}$ proceeds as follows. Given the kth iteration $\mathbf{x}^k$, the ith coordinate of $\mathbf{x}^{k+1}$ is

$$x_i^{k+1} = \arg\min_{y \in \Omega} F(x_1^{k+1}, ..., x_{i-1}^{k+1}, y, x_{i+1}^{k}, ..., x_n^{k}), \tag{11}$$

where Ω is the domain of possible values y can take. A given iteration is complete when this minimization has been performed for all coordinates i. Note in the equation above, the coordinates are minimized in ascending order beginning with x_1, however, any ordering that traverses all coordinates may be used.

In this optimization scheme, each coordinate of $\mathbf{x}$ corresponds to the phase correction of a single pulse. The optimization is performed by minimizing some cost function F for each coordinate/contribution. The cost functions examined are given below. One descent iteration consists of performing this process at each coordinate to minimize the cost function.

The coordinate descent method differs from a *gradient descent* method (also known as *steepest descent*) where optimization is performed by steps proportional to the negative of the gradient at each point. Because $\mathbf{x}$ has cardinality equal to the number of pulses contributing to the backprojected pixel sums (i.e., a large number), a gradient descent method could be computationally prohibitive. However, it can be shown that the sequence of Eq. 10 has similar convergence properties to the gradient descent method [11].

An important note when optimizing a group of pixels is that the same phase correction is applied to every sample at a given pulse. This means that a given group of pixels, termed a "tile," must be kept small enough that the same approximate phase error can be removed from each. For per-pulse radar system phase errors, this is the case for all samples in a given pules. For motion related phase errors, the tile size is a function of the slant-range to the tile and the expected magnitude of the motion errors. The result is tiles that are wide in azimuth (to examine the range migration curve of many targets with overlapping range migration curves) but possibly narrow in range (to obtain an accurate phase error estimate where the phase error is approximately the same across the given range swath).

This autofocus method is advantageous because it requires no general assumptions of platform motion in order to operate. Other methods of autofocus typically only operate on spotlight mode data. This is because of underlying assumptions made in the derivation of the autofocus algorithm. For example, many methods examine the azimuth spectrum of the formed image in order to determine the phase correction that should be applied. However, this assumes that the azimuth direction and the along-track direction are equivalent (i.e., orthogonal to the range or cross-track dimensions). This is certainly true for many flight geometries, but is not true in the case of an aircraft circling around a stationary point on the ground. For this case, a more general autofocusing method is required.

B. Cost functions

Although there are many reasonable cost functions that may be used for the purpose of optimization, our analysis is limited to three cases: maximum contrast, minimum entropy, and elliptic projection maximum contrast.

The maximum contrast method takes the form [12]

$$F = -\sum_{m \in \mathcal{M}} a_m^2. \tag{12}$$

This method maximizes the L^2-norm of the pixel or tile.

Maximum contrast methods have previously been shown to be particularly well suited for use in SAR because they maintain a good balance between high and low return areas [13]. "Furthermore, this metric has been shown to produce phase error estimates equivalent to maximum likelihood estimates under particular conditions" [14].

The minimum entropy method has the form [12]

$$F = -\sum_{m \in \mathcal{M}} a_m \log a_m. \tag{13}$$

Finally, the elliptic projection method is given as an analytic solution to an elliptic projection of the solution space to also maximize contrast. It is based on the work of [9]. We term this method the elliptic or Ash method.

C. Drift Compensation

The previous analysis for estimating phase error assumes that the correct range-compressed sample contributing to a given target / pixel is chosen for every pulse in the backprojection summation. This requires aircraft position measurements to be accurate to at least the same order of magnitude as the resolution cell. If the measurement errors are zero-mean with low variance then the correct samples are still chosen on average (resulting in good autofocus performance). Problems occur when the zero-mean/low-variance assumption is violated. An example of this is drift in the position measurement.

Position drift is common in measurements made by IMUs. As these sensors integrate measurements from accelerometers, drift is almost unavoidable. A key figure of merit in judging the quality of IMUs is the amount of drift a given IMU will present over a given period of time. If the drift over a given azimuth aperture is small then the correct range samples are still chosen, but if it grows larger then incorrect samples are used in the backprojection sum. Particularly troublesome is drift in the along-track direction as it leads to larger errors in estimation of the range to target than drift in the lateral directions.

One method for removing these problems is to estimate the position measurement drift. This can be performed similarly to the maximum contrast coordinate descent method described above. A bounded optimization is performed on the drift estimate, calculating the amount of drift that maximizes the L^2 norm of a given pixel or group of pixels. Note that drift is a first order effect, but a similar approach could be used to estimate higher-order motion errors if *a priori* knowledge of the presence such errors exists.

In general, several iterations may be required in order to descend on the optimal drift values. As shown previously, if the true platform motion is perfectly straight in range and elevation then there is no unique solution providing the position of the target (i.e., the optimization may converge to a drift in elevation / azimuth that is not correct). However, perfect platform motion is not generally the case for airborne imagery.

After the position drift is estimated, the antenna positions are updated accordingly. Note that this only removes the linear trend in the estimate error. Other motion errors are still present but are now zero mean. This means that on the average the correct range to target is used for every pulse and thus the correct range samples are selected in the backprojection sum. The aforementioned autofocus method may now be used to remove any remaining phase errors.

These results are only briefly given here to show that drift doesn't cause catastrophic failure of this autofocus method. A more rigorous derivation as well as other motion related effects are given in a future paper.

IV. Results

The elliptic method provides an analytic estimate of the phase error for each pulse throughout a coordinate descent iteration. However, the maximum contrast and minimum entropy methods require a numerical method to estimate the phase error at each pulse. To do this, we perform a scalar bounded minimization from $-\pi \leq \hat{\phi}_e \leq \pi$ using Brent's method [15]. Brent's method is a root-finding algorithm which

Table II
SIMULATION PARAMETERS

Parameter	Value
Wavelength	0.3 m
Azimuth beamwidth	0.3 rad
Along-track velocity	50 m/s
PRF	200 Hz
TX bandwidth	300 MHz

combines several methods (bisection method, secant method, and inverse quadratic interpolation). It is as reliable as the bisection method but can be as computationally efficient as the less reliable methods.

The drift compensating algorithm, on the other hand, must find a vector of three coordinates, not a scalar value. An attempt was made to use Brent's method on each coordinate individually, but resulted in poor convergence. Instead, we use a modification of Powell's method [16], [17], which is a conjugate direction method. We found that it had the best convergence results of any method examined. Other methods tested include sequential least squares, the Nelder-Mead method [18], [19] (uses the Simplex algorithm), the Polak-Ribiere [20] (a nonlinear conjugate gradient algorithm), and the Broyden, Fletcher, Goldfarb, and Shanno method [21] (a quasi-Newton method using only first derivatives).

Simulated data sets are created using the specifications in Table II. For results requiring zero mean gaussian noise be added to the position estimates, a variance of 0.1 m at every pulse was used. For results requiring drift, 1.5 m/s in the along-track direction (1/50 the forward velocity) and 2 cm/s in the cross-track direction were used. These values were arbitrarily chosen and represent drift values well beyond those expected with a reasonable IMU/GPS combined INS.

Figure 2 compares the performance of the various autofocus cost functions on a simulated stripmap data set, where the antenna positions have random gaussian noise added. Only one iteration of autofocusing is performed. We select a range cell migration curve of a range compressed point target from the simulation and plot the backprojected phase error (in radians) at every pulse. The original backprojected data without autofocus exhibits a large amount of phase error. After autofocusing using the elliptic/Ash method, the phase error is reduced significantly. The maximum contrast and minimum entropy methods both show even more reduction in phase error, with the minimum entropy solution performing slightly better.

Figure 3 shows the backprojected images of the simulated data set using a single iteration with each of the autofocusing methods. Two targets are present at this location in the data. Plot (a) shows the original backprojected image without any autofocusing. Because of the large phase error present, the targets are blurred in range and particularly in azimuth. Plot (b) shows the result of autofocusing using the Ash/elliptic method. The blurring is significantly reduced and the individual point targets are now distinguishable, however some spreading of the azimuth energy is still noticeable. This corresponds to the phase error remaining after autofocusing as seen in the previous figure. The plot in (c) demonstrates focusing using the

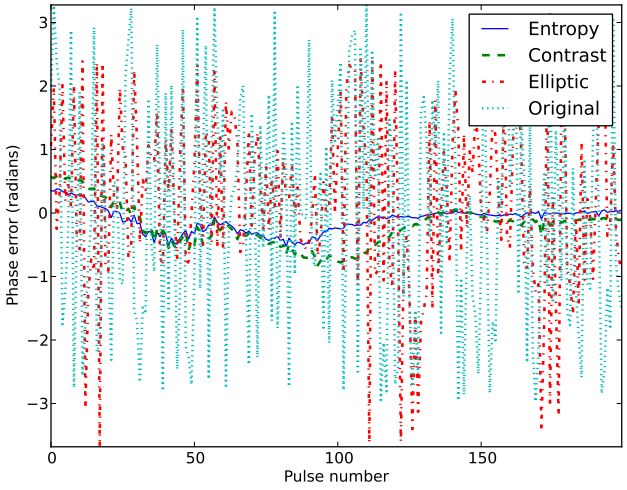

Figure 2. Plot showing phase error at each pulse corresponding to the peak

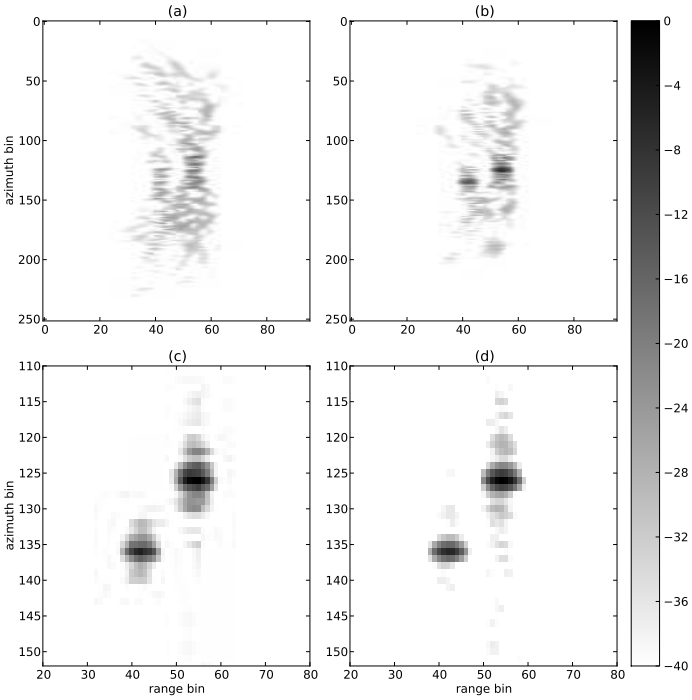

Figure 3. Backprojected images in dB of simulated data with two point targets. (a) shows the original image and (b-d) show autofocused results for various cost functions: (b) elliptic, (c) maximum contrast, and (d) minimum entropy.

maximum contrast method and (d) demonstrates the minimum entropy method. Note that the axes have been zoomed on these two images to show more detail. These methods show similar levels of performance, although the side lobes are lower with the minimum entropy method.

These features are more easily seen in Figure 4 which contains an azimuth slice through one of the point targets. In (a) the three autofocus methods are plotted together and in (b) the central region around the main lobe is zoomed. The lobe peak and width is nearly identical for both the maximum contrast and minimum entropy methods.

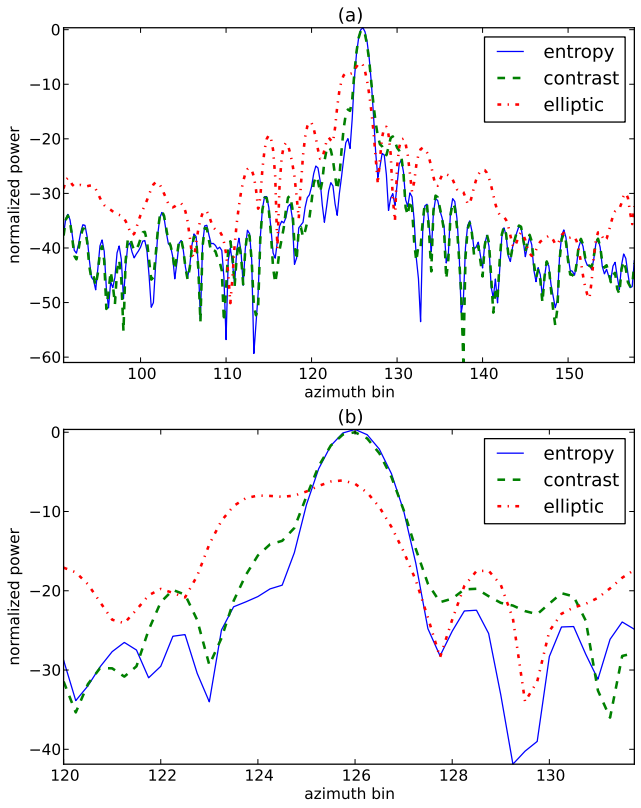

Figure 4. Azimuth slices through one of the autofocused point targets from Fig. 3 for each autofocus cost function. The lower plot (b) shows a zoomed-in region around the central peak.

V. Conclusion

This paper presents an autofocus method congruent with the SAR backprojection image formation algorithm. The paper discusses the motivation for developing a new autofocus method and what the problems are that necessitate autofocus. The autofocus method is developed which is an estimation based method that utilizes a coordinate descent framework with various cost functions to find an optimal phase correction at each pulse. Thus, this autofocus method is well suited to backprojection and its versatile imaging geometries.

References

[1] W. Carrara, R. Goodman, and R. Majewski, *Spotlight Synthetic Aperture Radar: Signal Processing Algorithms*. Norwood, MA: Artech House, 1995.

[2] C. Mancill and J. Swiger, "A map drift autofocus technique for correcting higher-order SAR phase errors," in *27th Annual Tri-Service Radar Symposium Record*, 1981, pp. 391–400.

[3] P. Eichel, D. Ghiglia, C. Jakowatz Jr *et al.*, "Speckle processing method for synthetic-aperture-radar phase correction," *Optics Letters*, vol. 14, no. 1, pp. 1–3, 1989.

[4] D. E. Wahl, P. H. Eichel, D. C. Ghiglia, and J. Jakowatz, C. V., "Phase gradient autofocus-a robust tool for high resolution SAR phase correction," *IEEE T Aero Elec Sys*, vol. 30, no. 3, pp. 827–835, 1994.

[5] S. A. S. Werness, W. G. Carrara, L. S. Joyce, and D. B. Franczak, "Moving target imaging algorithm for SAR data," *IEEE T Aero Elec Sys*, vol. 26, no. 1, pp. 57–67, 1990.

[6] M. I. Duersch and D. G. Long, "Analysis of MIMO pixel correlation in SAR," in review (IEEE Trans. Geosci. Remote Sens.).

[7] M. A. Richards, *Fundamentals of Radar Signal Processing*. McGraw-Hill, 2005.

[8] R. L. Morrison, M. N. Do, and D. C. Munson, "SAR image autofocus by sharpness optimization: A theoretical study," *IEEE T Image Process*, vol. 16, no. 9, pp. 2309–2321, 2007.

[9] J. N. Ash, "An autofocus method for backprojection imagery in synthetic aperture radar," *IEEE Geosci. Remote. S.*, vol. 9, no. 1, pp. 104–108, 2012.

[10] T. Moon and W. Stirling, *Mathematical methods and algorithms for signal processing*. Prentice hall, 2000, vol. 204.

[11] J. C. Bezdek, R. J. Hathaway, R. E. Howard, C. A. Wilson, and M. P. Windham, "Local convergence analysis of a grouped variable version of coordinate descent," *Journal of Optimization Theory and Applications*, vol. 54, pp. 471–477, 1987.

[12] L. Xi, L. Guosui, and J. Ni, "Autofocusing of ISAR images based on entropy minimization," *IEEE T Aero Elec Sys*, vol. 35, no. 4, pp. 1240–1252, 1999.

[13] J. Fienup and J. Miller, "Aberration correction by maximizing generalized sharpness metrics," *J. Opt. Soc. Am.*, vol. 20, no. 4, pp. 609–620, 2003.

[14] T. J. Schulz, "Optimal sharpness function for SAR autofocus," *IEEE Signal Proc Let*, vol. 14, no. 1, pp. 27–30, 2007.

[15] R. Brent, *Algorithms for Minimization Without Derivatives*. Englewood Cliffs, NJ: Prentice-Hall, 1973, ch. 3-4.

[16] M. Powell, "An efficient method for finding the minimum of a function of several variables without calculating derivatives," *The computer journal*, vol. 7, no. 2, pp. 155–162, 1964.

[17] W. Press, B. Flannery, S. Teukolsky, W. Vetterling *et al.*, *Numerical recipes*. Cambridge Univ Press, 1986.

[18] J. A. Nelder and R. Mead, "A simplex method for function minimization," *The Computer Journal*, vol. 7, no. 4, pp. 308–313, 1965.

[19] M. Wright, "Direct search methods: Once scorned, now respectable," *Pitman Research Notes in Mathematics Series*, pp. 191–208, 1996.

[20] E. Polak, *Computational Methods in Optimization: a Unified Approach*. Academic Press, 1971, vol. 77.

[21] J. Nocedal and S. Wright, *Numerical Optimization*. Springer, 2006.